The influence of dynamic characteristics of six-bar linkage mechanical press transmission system on the accuracy of slider

ZHAI Hua[1,a] *, ZHANG Yingjie[1,b], SONG Zhaoai[1,c], ZANG Congyun[2,d], ZHANG QingLin[2,e], LV Pin[3,f] and LI Jiajie[1,g]

[1]Anhui Province Key Lab of Aerospace Structural Parts Forming Technology and Equipment, Hefei University of Technology

[2]Jiangsu CPTEK Servo Technology Co.,Ltd., Liyang, 213300, China

[3]Tai'an Hualu Forging Machine Tool Co., Ltd., Taian, 271000, China1 Heidelberg, Germany

[a]jxzhaihuajx@hfut.edu.cn, [b]zyjcq@foxmail.com, [c]2304655692@qq.com, [d]zangchongyun@cptek.com.cn, [e]zhangqinglin@cptek.com.cn, [f]lupin@hfut.edu.cn, [g]2022170266@mail.hfut.edu.cn

Keywords: Six Link Mechanical Press, Dynamic Model, Drive System, Dynamic Characteristis, Orthogonal Experimental Method

Abstract. The six-bar linkage mechanical press is a crucial equipment in the preparation of metal bipolar plates for fuel cells. The dynamic characteristics of the transmission system have a significant impact on the precision of the slide operation, which directly affects the quality of the bipolar plate forming. In this article, A dynamic model of the six-bar linkage transmission system under complex forming workloads was established to research dynamic characteristics. The dynamic characteristics of each bar was analyzed under load conditions. Combining with the orthogonal experimental method, we investigate the various parameters influence on the press slide precision. Through an six-factor orthogonal experiment, the results show that the down-push rod dynamic characteristics are the most important factor affecting the slide stroke precision under the transmission system's workload conditions. Therefore, it is necessary to optimize the down-push rod design and manufacturing process. The results of this study have a certain reference value for the design and optimization of the six-bar linkage mechanical press, and the improvement of the quality of metal bipolar plate preparation for fuel cells.

Introduction

As a critical component within the fuel cell framework, the metal bipolar plate facilitates pivotal functions such as the direction of reactive gases, current guidance, provision of structural support, drainage, and acting as a cooling component[1]. The six-bar mechanical press is a significant apparatus in the fabrication of fuel cell metal bipolar plates, with the dynamical characteristics of its transmission system having a profound impact on the precision of the slider operation, thereby directly influencing the forming quality of the bipolar plates[2].In the analysis of mechanisms, the dynamic force and positioning accuracy of mechanical presses are crucial [3]. Some scholars have pointed out that factors such as clearance, friction, stiffness, and geometric deviation have significant impacts on them [4-6]. Numerous simulations and experiments [7-11] have also confirmed that compared to the rigid model, the rigid-flexible coupling model considering clearance and lubrication fits better with experimental data. The existence of clearance and friction as well as the stress deformation of the connecting rods can significantly affect the dynamic characteristics and slider accuracy of the press. Some scholars [12-14] have considered the reliability of dynamic accuracy for multi-clearance multi-connecting rod, and improved the dynamic accuracy of mechanical presses through comprehensive optimization of mathematical models, closed-loop control, and other methods.

This manuscript focuses on the six-bar mechanical press, establishes a simulated dynamic model for the six-bar mechanism. It explores the deformation and strain of each bar post load application, and with the orthogonal experimental method, the impact of parameters post deformation under force on the operational precision of the press slider has been improved.

Construction and analysis of the simulated dynamic model for the six-bar mechanism

Construction of the kinematic model for the six-bar mechanism. The kinematic relationship of the six-bar mechanism is illustrated in Fig. 1. The primary design parameters of the six-bar mechanism include the crank length L1, the pull rod length L2, the lengths of the two sides of the triangle frame L3 and L4, the push rod length L5, the fixed point coordinates x and y connecting the triangle frame and the machine frame , the slider offset e, and the angle between the two sides of the triangle frame θ. When these parameters are fixed, the kinematic trajectory of the entire mechanism is fully determined. The kinematic expression of the six-bar mechanism is shown in Eq. 1. By substituting the parameters in Table 1 for calculation, the slider stroke curve shown in Fig. 2 can be obtained.
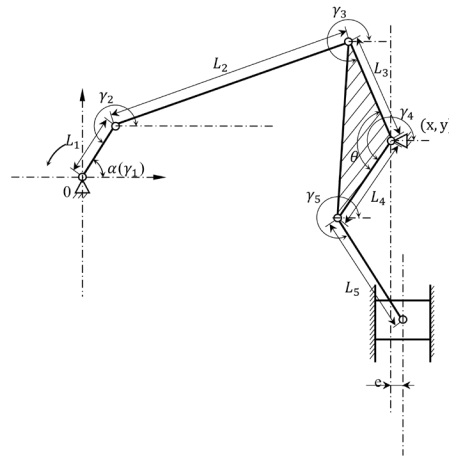

Fig. 1. Schematic diagram of the kinematic relationship of the six-bar mechanism.

The variable γ_i represents the angle between each rod and the horizontal direction, while S corresponds to the y-component of the slider's coordinates.

Table 1. Parameter specific values.

Parameter	Value
L_1/mm	113
L_2/mm	1000
L_3/mm	330
L_4/mm	270
L_5/mm	500
x/mm	1050
y/mm	100
e/mm	0
θ/°	134

$$\begin{cases} L_1 \cos\gamma_1 + L_2 \cos\gamma_2 + L_3 \cos\gamma_3 - x = 0 \\ L_1 \sin\gamma_1 + L_2 \sin\gamma_2 + L_3 \sin\gamma_3 - y = 0 \\ \quad x + L_4 \cos\gamma_4 + L_5 \cos\gamma_5 - e = 0 \\ \quad y + L_4 \sin\gamma_4 + L_5 \sin\gamma_5 - S = 0 \end{cases} \quad (1)$$
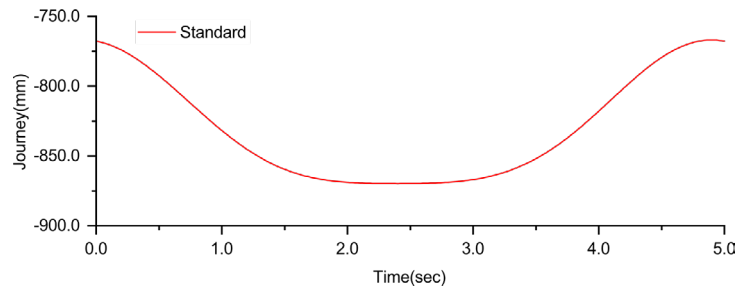
Fig. 2. Standard stroke curve.

Under the assumption that only the kinematic constraints between the links are considered, neglecting factors such as the deformation of the links and clearances at the hinge points, it can be assumed that the motion of the slider is perfectly accurate. Therefore, the trajectory of the slider under this ideal condition can be taken as the reference.

Establishment of dynamic model of six-link multi-flexible body simulation. Using dynamic analysis software software, a simulation model of a six-bar linkage can be established. Rotational joint constraints are set at each hinge point, while a translational joint constraint is set at the slider. All the linkages except the slider of the six-link mechanism are flexibly processed. The crank rotates at a speed of 72 degrees per second. When the slider reaches the loading point, an upward load of 80 tons is applied. When the slider reaches the unloading point, the load force is removed. The loading point is located 20 mm above the bottom dead center, while the unloading point is located 1mm above the bottom dead center. The cross-section of each link is a rectangular shape with dimensions of 40 mm × 40 mm.

Based on the provided conditions and procedures, the simulation model is configured, and solving the model yields the slider's displacement curve under working load as well as the deformation and force results for each link. As shown in Fig. 3 below, it presents a comparison between the slider's displacement curve considering the deformation of the six-bar linkage mechanism and the standard displacement curve.
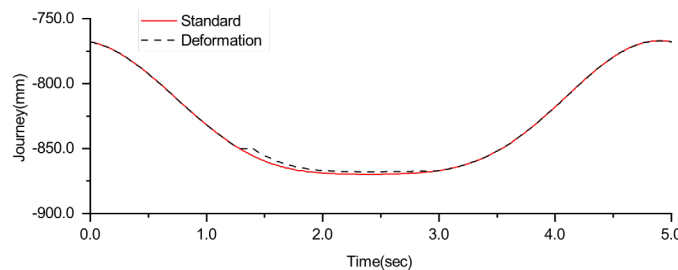

Fig. 3. Comparison diagram of load slide block stroke and standard stroke.

From Fig. 3, there is a certain difference between the slider's displacement under load and the standard displacement curve. This indicates that the dynamic characteristics of the transmission system after being loaded have a significant influence on the operational precision of the slider. Furthermore, it can be observed that after reaching the loading point where the load force is applied, the slider's displacement remains unchanged for a period of time. This implies that during this period, the six-bar linkage begins to undergo elastic deformation due to the applied load force, which is the main reason for the change in slider precision. Due to the applied load force, the six-bar linkage mechanism remains in a state of compression deformation as it operates between the load point and the unloading point. If the overall stiffness of the six-bar linkage mechanism is insufficient, it may lead to instances where the slider starts its return stroke before reaching the

unloading point and the bottom dead center. This significantly reduces the formed product quality of the six-bar linkage mechanical press.

Analysis of the influence of the deformation of each connecting rod on the running accuracy of the slider

Deformation and condition of each bar under load. Based on the meticulous analysis of the multi-body soft-body dynamics simulation, the deformation and force distribution of each link under the load conditions are illustrated in Fig. 4 and Fig. 5, respectively.
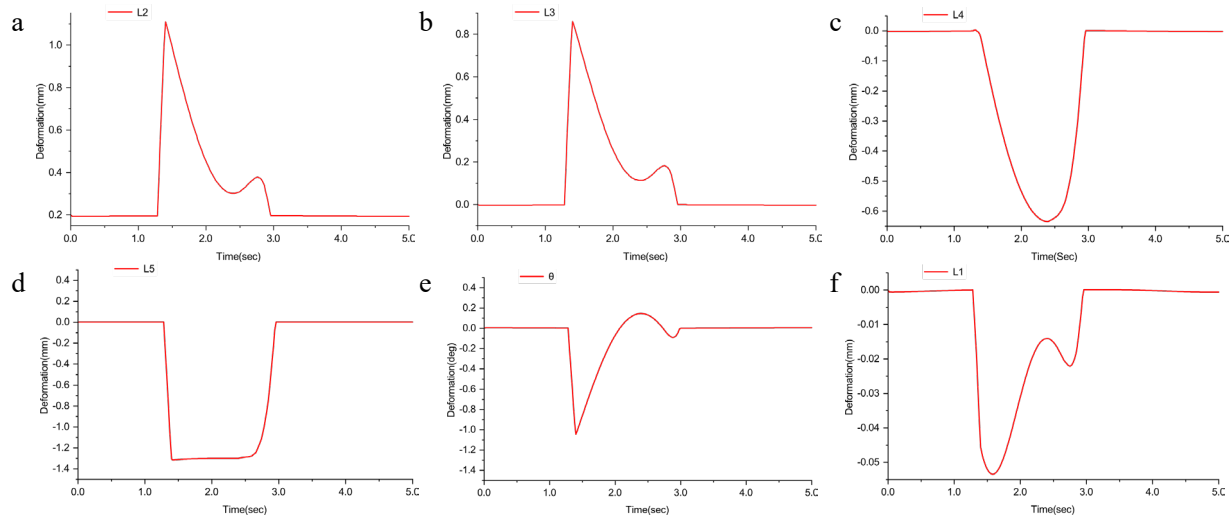

Fig. 4. Deformation diagram of each connecting rod under load. (a) L1 bar load deformation diagram; (b) L2 bar load deformation diagram; (c) L3 bar load deformation diagram; (d) L4 bar load deformation diagram; (e) L5 bar load deformation diagram; (f) θ angle load deformation diagram.
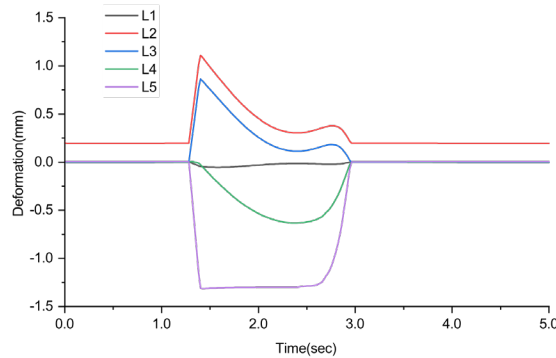
Fig. 5. Comparison diagram of load deformation of each connecting rod.

From Fig. 4 and Fig. 5, The slider causes the maximum deformation in link L5, and the triangular frame also undergoes deformation in terms of its angle. Additionally, the maximum deformation of each link in the six-bar mechanism at the point of force application and the deformation of each link at the bottom dead center position can be determined. By utilizing the formula for strain calculation, the strain values for each link can be obtained and are presented in Table 2.

Table 2. Results of deformation and strain of each bar under loading.

NO.	Maximum deformation at the load point /mm	Maximum strain at the load point	Deformation at the lower dead point /mm	Strain at the lower dead point
L1	-0.0532	-0.4708×10^{-3}	-0.0142	-0.1257×10^{-3}
L2	1.1091	1.1091×10^{-3}	0.3038	0.3083×10^{-3}
L3	0.8617	2.6112×10^{-3}	0.1139	0.3452×10^{-3}
L4	-0.6344	-2.3496×10^{-3}	-0.6298	-2.3326×10^{-3}
L5	-1.3154	-2.6308×10^{-3}	-1.293	-2.586×10^{-3}

Likewise, the maximum deformation at the load point for the angle θ is -1.0429°, with a corresponding maximum strain of -7.78×10^{-3}. At the bottom dead center position, the deformation is 0.1431°, and the strain is 1.0679×10^{-3}. Based on the analysis presented in Table 2, it can be concluded that under the loaded condition, link L5 exhibits the highest deformation and strain at both the point of force application and the bottom dead center position.

Analysis of the Influence of rod deformation on the accuracy of slider load point. Six-bar linkage mechanism undergoes deformation of its members when subjected to loading at the position of the load point. In comparison to the standard stroke curve, the slider exhibits a phenomenon of lagging behind as it crosses the load point. This lagging phenomenon results in the crank reaching a specific phase while the slider fails to reach its ideal position during the interval between the slider's movement from the load point to the unloading point, thereby reducing the precision of slider motion.

The numerical values of the maximum deformation of each member at the load point can be obtained from Table 2. The results have shown that when considering only the tensile and compressive stiffness of each member, increasing the stiffness of the members of the six-bar linkage mechanism in various ways will result in a decrease in the maximum deformation of each member at the load point. Additionally, different combinations of stiffness values for each member correspond to a set of maximum deformations for the members, as shown in Eq. 2.

$$f(E_1, E_2, E_3, E_4, E_5) = [\Delta L_1, \Delta L_2, \Delta L_3, \Delta L_4, \Delta L_5] \tag{2}$$

Where, E_i is the stiffness of each bar, while ΔL_i denotes the maximum deformation of each bar at the location of load. When only the stiffness of each bar of the given six-bar mechanism is increased, the maximum deformation of each bar at the load point exhibits a relationship as depicted in Eq. 3.

$$|\Delta L_i| < |\Delta L_{i0}| \tag{3}$$

Where, ΔL_{i0} represents the maximum deformation of each bar at the point of load under the state given in Section Establishment of dynamic model of six-link multi-flexible body simulation, as shown in Table 2.

Using the phase angle φ_0 at the point of load when the slider runs to the standard stroke as the reference value, we take the intermediate value ΔL_i between the static state and the maximum deformation value in Table 2 in the six-bar linkage mechanism, and add it to the initial parameters in Table 1 as the design value of the bar length of the six-bar linkage mechanism. At this design value, we calculate the phase angle φ of the crank when the slider runs to the load position under the rigid state. By comparing the difference $\Delta\varphi$ between this phase angle φ and the phase angle φ_0 obtained at the standard stroke, the accuracy of the load point under the stiffness E_i of the slider can be compared with the selected intermediate value ΔL_i as the corresponding maximum deformation at the load point.

An analysis of the influence of the accuracy of the slider's load point on various link deformations can be conducted using the orthogonal experimental method. The orthogonal experimental method is a statistical experimental design method used to study the influence of multiple factors on the response variable. Compared with the method of full factorial full level experiments, orthogonal experimental method can determine the main factors that affect the experimental indicators through fewer experiments [15-17]. By employing a special design matrix (orthogonal table), this method can effectively evaluate the main factors and interaction effects within a limited number of experimental trials.

First, the assessment index is established as the difference $\Delta\varphi$ between the phase angle φ of the load point position under different factors and the phase angle φ_0 of the load point under the standard stroke.

Secondly, only the influence of link deformations on the accuracy of the slider's load point is considered, and the main factors are determined to be: L1, L2, L3, L4, and L5. The reference parameters are as shown in Table 1, with each parameter having an offset range of $[0, \Delta L_{i0}]$. As obtained from the aforementioned simulation, the phase angle $\varphi_0 = 122.16°$ of the load point under the standard stroke is determined.

Considering that the included angle θ of the triangle rod is one of the design values and also varies under load, θ is likewise considered as an auxiliary factor. Therefore, there are a total of 6 factors, and to ensure greater accuracy in the analysis results, each factor is divided into 5 levels. It is finally decided to use the orthogonal table $L_{25}(5^6)$, as shown in Table 3.

Table 3. $L_{25}(5^6)$ Orthogonal table.

NO.	Factor A	Factor B	Factor C	Factor D	Factor E	Factor F
1	1	1	1	1	1	1
2	1	2	3	4	5	2
3	1	3	5	2	4	3
4	1	4	2	5	3	4
5	1	5	4	3	2	5
6	2	1	5	4	3	5
7	2	2	2	2	2	1
8	2	3	4	5	1	2
9	2	4	1	3	5	3
10	2	5	3	1	4	4
11	3	1	4	2	5	4
12	3	2	1	5	4	5
13	3	3	3	3	3	1
14	3	4	5	1	2	2
15	3	5	2	4	1	3
16	4	1	3	5	2	3
17	4	2	5	3	1	4
18	4	3	2	1	5	5
19	4	4	4	4	4	1
20	4	5	1	2	3	2
21	5	1	2	3	4	2
22	5	2	4	1	3	3
23	5	3	1	4	2	4
24	5	4	3	2	1	5
25	5	5	5	5	5	1

The levels corresponding to each factor are shown in Table 4.

Table 4. Factor and level comparison table.

Level	L1 A	L2 B	L3 C	L4 D	L5 E	θ F
1	-0.0106	0.2218	0.1725	-0.1269	-0.2631	-0.2086
2	-0.0213	0.4436	0.3447	-0.2538	-0.5262	-0.4172
3	-0.0319	0.6655	0.5170	-0.3806	-0.7892	-0.6257
4	-0.0426	0.8873	0.6894	-0.5075	-1.0523	-0.8343
5	-0.0532	1.1091	0.8617	-0.6344	-1.3154	-1.0429

Based on Table 3 and Table 4, conduct the experimental design, calculate the phase angle differences for each experimental combination, and enter the results into the right-hand column of the table, as shown in Table 5.

Table 5. Experimental data.

NO.	A	B	C	D	E	F	$\Delta\varphi$
1	1	1	1	1	1	1	1.296
2	1	2	3	4	5	2	4.032
3	1	3	5	2	4	3	4.032
4	1	4	2	5	3	4	4.896
5	1	5	4	3	2	5	5.04
6	2	1	5	4	3	5	5.04
7	2	2	2	2	2	1	1.872
8	2	3	4	5	1	2	2.736
9	2	4	1	3	5	3	4.608
10	2	5	3	1	4	4	4.752
11	3	1	4	2	5	4	4.896
12	3	2	1	5	4	5	5.616
13	3	3	3	3	3	1	2.592
14	3	4	5	1	2	2	5.216
15	3	5	2	4	1	3	3.456
16	4	1	3	5	2	3	3.6
17	4	2	5	3	1	4	3.6
18	4	3	2	1	5	5	5.472
19	4	4	4	4	4	1	3.312
20	4	5	1	2	3	2	3.168
21	5	1	2	3	4	2	3.312
22	5	2	4	1	3	3	3.456
23	5	3	1	4	2	4	4.176
24	5	4	3	2	1	5	4.32
25	5	5	5	5	5	1	3.888
K_{1j}^{avr}	3.8592	3.6288	3.7728	4.0384	3.0816	2.592	
K_{2j}^{avr}	3.8016	3.7152	3.8016	3.4848	3.7504	3.6928	
K_{3j}^{avr}	4.3552	3.8016	3.8592	3.8304	3.8304	3.8304	
K_{4j}^{avr}	3.8304	4.4704	3.888	4.0032	4.2048	4.464	
K_{5j}^{avr}	3.8304	4.0661	4.3552	4.5216	4.5792	5.0976	
R_j	0.5536	0.8416	0.5824	1.0368	1.4976	2.5056	

In order to assess the impact of various factor levels on performance indicators, the phase angle differences at all levels of factor j under level i are summed and divided by the number of levels, yielding the average of the experimental indicators at level i of factor j. The calculation process at level 1 of factor A is illustrated in Eq. (4).

$$K_{1A}^{avr} = \frac{1}{5}(1.296 + 4.023 + 4.023 + 4.896 + 5.04) = 3.8592 \qquad (4)$$

The calculated results K_{ij}^{avr} and R_j should be filled into the corresponding positions in Table 5.

We conducted a sorting of the obtained range R_j, and thereby established the primary and secondary relationships of the factors' impact on the indicators.

$$F \rightarrow E \rightarrow D \rightarrow B \rightarrow C \rightarrow A \qquad (5)$$

Analysis of the primary and secondary relationships reveals that, apart from the auxiliary factor of the angle φ of the tripod, under the load condition, the push rod L5 has the most significant impact on the accuracy of the point of load.

We divided the range R_j by the interval ε_i at the horizontal of the response factor (as shown in Table 6) to obtain the unit deformation range R_{i0} (as depicted in Table 6).

Table 6. Unit deformation range table.

Factor	Range R_j	Level interval ε_j	Unit deformation range R_{j0}
A	0.5536	0.01064	52.0331
B	0.8416	0.22182	3.7941
C	0.5824	0.17254	3.3754
D	1.0368	0.12688	8.1715
E	1.4976	0.26308	5.6927
F	2.5056	0.20858	12.0127

The analysis of Table 6 reveals that, apart from the auxiliary factor F, the deformation of the crank under unit deformation has a significantly higher impact on the accuracy of the slider's capacity to occur than the deformation of other rods. However, under general loading conditions, the crank is relatively short and experiences much smaller forces compared to other components, resulting in deformation far smaller than that of the other rods under the same tensile and compressive stiffness. Therefore, the impact on the accuracy of the slider's load point is not as significantly as that of the push rod L5.

Analysis of the impact of increased rod stiffness on the accuracy of slider movement. The deformation of each rod has a significant impact on the accuracy of slider movement. We investigated the influence of increased rod stiffness on the accuracy of slider movement by separately enhancing the stiffness of each rod in the simulation model. According to the stiffness calculation formula, the stiffness of a rod can be altered by modifying its cross-sectional area. Therefore, we increased the stiffness of each rod by sequentially changing the cross-sectional area from 30 mm×30 mm to 100 mm×100 mm in the simulation model. Subsequently, we conducted simulation calculations to obtain the travel curves of the slider after the stiffness of each rod was increased, as well as the travel curves of the slider after the stiffness of all rods was increased, as depicted in Fig. 6.
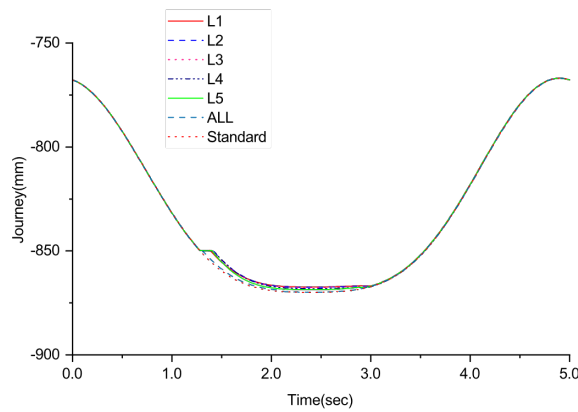
Fig. 6. Comparison diagram of stroke after change of stiffness of different connecting rod.

In Fig. 6, L1-L5 respectively represent the travel curves of the slider after the corresponding connecting rod stiffness is increased, while ALL represents the travel curve of the slider after all rod stiffness are increased, and standard represents the standard travel curve of the slider. Analysis of Fig. 6 reveals that after altering the stiffness of each slider, the travel curves in the unloaded travel segment are generally consistent, whereas in the loaded travel segment, significant differences are observed among the respective curves. The travel curves of each slider in the loaded travel segment are illustrated in Fig. 7.
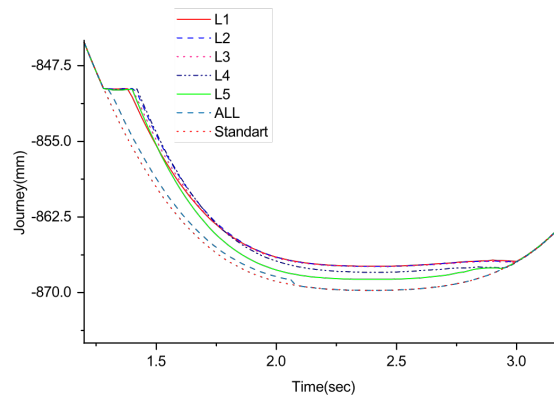

Fig. 7. Comparative diagram of loading stroke after the change of different connecting rod stiffness.

From Fig. 7, apart from the travel curve of the slider after increasing the stiffness of all connecting rods, the travel curve of the slider after increasing the stiffness of the push rod L5 closely approximates the standard curve during the loaded travel segment. Hence, it can be inferred that increasing the stiffness of the push rod L5 effectively enhances the operational precision of the slider. Compared to enhancing the stiffness of the push rod L5, increasing the stiffness of the crank can effectively ameliorate the lag phenomenon in the slider's movement when reaching the load point. Similarly, it has been observed that after enhancing the stiffness of all rods, there is a notable improvement in the operational precision of the slider during the loaded travel segment, and the slider has gained the capability to traverse the unloading point and reach the bottom dead center. Enhancing the overall stiffness of the six-bar linkage mechanism is an effective approach to address the inability of the slider to traverse the unloading point and reach the bottom dead center.

Conclusion

1) The dynamic characteristics of the six-bar linkage mechanical press transmission system significantly impact the precision of the slide motion.

2)   Among the members of the six-bar linkage mechanism, the lower connecting rod L5 has the most significant influence on the accuracy of the capacity location after being subjected to loading.

3)   The crank rod deformation in the six-bar linkage mechanism has the greatest impact on the precision of the capacity location of the slide.

4)   Enhancing the stiffness of the lower connecting rod L5 in the six-bar linkage mechanism can effectively improve the precision of the slide motion.

5)   Increasing the stiffness of the crank L1 can effectively ameliorate the lag phenomenon occurring when the slide reaches the capacity location.

6)   Enhancing the overall stiffness of the six-bar linkage mechanism is an effective approach to address the phenomenon where the slide fails to pass the unloading point and reach the bottom dead center.

Acknowledgements

References

[1] X. Li, I. Sabir, Review of bipolar plates in PEM fuel cells:flow-field designs, Int. J. Hydrogen Energy 30 (2005) 359-371. https://doi.org/10.1016/j.ijhydene.2004.09.019

[2] M. Xiao, G. Geng, G. Li, H. Li, R. Ma, Analysis on dynamic precision reliability of high-speedprecision press based on Monte Carlo method, Nonlinear Dynamics 90 (2007) 2979-2988. . https://doi.org/10.1007/s11071-017-3857-7

[3] V.V. Telegin, A.M. Kozlov, V.I. Sakalo, Solid modeling and dynamic analysis of mechanisms of press-forging machines, Procedia Eng. 206 (2017) 1258-1263. https://doi.org/10.1016/j.proeng.2017.10.628

[4] Z. Chval, M. Cechura, Optimization of power transmission on mechanical forging presses, Procedia Eng. 69 (2014) 890-896. https://doi.org/10.1016/j.proeng.2014.03.067

[5] N. Wagner, T. Päßle, Screening-based evidence of the impact of geometrical deviations on inner   stresses on mechanical press, Procedia Manuf. 27 (2019) 185-191. https://doi.org/10.1016/j.promfg.2018.12.063

[6] Q. Tiana, P. Flores, H.M. Lankaranic, A comprehensive survey of the analytical, numerical and experimental methodologies for dynamics of multibody check for updates mechanical systems with clearance or imperfect joints, Mechanism and Machine Theory 122 (2018) 1-57. https://doi.org/10.1016/j.mechmachtheory.2017.12.002

[7] O. Muvengei, J. Kihiu, B. Ikua, Numerical study of parametric effects on the dynamic response of planar multi-body systems with differently locted frictionless revolute clearance joints, Mechanism and Machine Theory 53 (2012) 30-46.

[8] Zheng Feng Bai, Yang Zhao, Dynamics modeling and quantitative analysis of multibody systems including revolute clearance joint, Precision Engineering 36 (2012) 554-576.

[9] P. Flores, R. Leine, C. Glocker, Modeling and analysis of rigid multibody systems with translational clearance joints based on the nonsmooth dynamics approach, Multibody Dynamics: Computational Methods and Applications 107-130 (2011).

[10] Xinyu Dong, Yu Sun, Xuze Wu, et al. Dynamic modeling and performance analysis of

toggle-linkage presses considering mixed clearances and flexibility, International Journal of Non-Linear Mechanics, 147 (2022) 104243.

[11] Y. Chen, Y. Sun, C. Chen, Dynamic analysis of a planar slider-crank mechanism with clearance for a high speed and heavy load press system, Mechanism and Machine Theory 98 (2016) 81-100.

[12] X. Chen, S. Gao, Dynamic accuracy reliability modeling and analysis of planar multi-link mechanism with revolute clearance, European J. Mech. A Solids 90 (2021) 104317. https://doi.org/10.1016/j.euromechsol.2021.104317

[13] F. Hoppe, C. Pihan, P. Groche, Closed-loop control of eccentric presses based on inverse kinematic models, Procedia Manuf. 29 (2019) 240-247. https://doi.org/10.1016/j.promfg.2019.02.132

[14] Y. Li, Y. Su, S. Wang, Dimensional synthesis for multi-linkage of high-speed mechanical press, Procedia Eng. 81 (2014) 1639-1644. https://doi.org/10.1016/j.proeng.2014.10.204

[15] Z. Yuan, X. Chen, H. Zeng, K. Wang, J. Qiu, Identification of the elastic constant values for numerical simulation of high velocity impact on dyneema® woven fabrics using orthogonal experiments, Compos. Struct. 204 (2018) 178-191. https://doi.org/10.1016/j.compstruct.2018.07.024

[16] S. Zhang, Y. Mao, F. Liu, H. Xu, Z. Qu, X. Liao, Multi-objective optimization and evaluation of PEMFC performance based on orthogonal experiment and entropy weight method, Energ. Convers. Manage. 291 (2023) 117310. https://doi.org/10.1016/j.enconman.2023.117310

[17] U. Karaguzel, M. Bakkal, E. Budak, Mechanical and thermal modeling of orthogonal turn-milling operatio, Procedia CIRP 58 (2017) 287-292.